RADAR

Research Archive and Digital Asset Repository

OXFORD
BROOKES
UNIVERSITY

PHILOSOPHICAL TRANSACTIONS B

Investigating mixotrophic metabolism in the model diatom *Phaeodactylum tricornutum*.

Valeria Villanova[1,2], Antonio Emidio Fortunato[3], Dipali Singh[5], Davide Dal Bo[2] Melissa Conte[2], Toshihiro Obata[4], Juliette Jouhet[2], Alisdair R. Fernie[4], Eric Marechal[2], Angela Falciatore[3], Julien Pagliardini[1], Adeline Le Monnier[1], Mark Poolman[5], Gilles Curien[2], Dimitris Petroutsos[2*], Giovanni Finazzi[2*]

[1]*Fermentalg SA, F-33500 Libourne, France.*
[2]*Laboratoire de Physiologie Cellulaire et Végétale, UMR 5168, Centre National de la Recherche Scientifique (CNRS), Commissariat à l'Energie Atomique et aux Energies Alternatives (CEA), Université Grenoble Alpes, Institut National Recherche Agronomique (INRA), Institut de Biosciences et Biotechnologies de Grenoble, (BIG), CEA Grenoble, F-38054 Grenoble cedex 9, France.*
[3]*Laboratoire de Biologie Computationnelle et Quantitative, Sorbonne Universités, UPMC, Institut de Biologie Paris-Seine, CNRS, 15 rue de l'Ecole de Médecine, Paris, 75006, France.*
[4]*Max-Planck Institut für Molekulare Pflanzenphysiologie, Am Mühlenberg 1, 14476 Golm-Potsdam, Germany.*
[5]*Department of Biological and Medical Sciences, Oxford Brookes University, Oxford, OX3 0BP, U.K.*

Main Text

Summary

Diatoms are prominent marine microalgae, interesting not only from an ecological point of view, but also for their possible use in biotechnology applications. They can be cultivated in phototrophic conditions, using sunlight as the sole energy source. Some diatoms, however, can also grow in a mixotrophic mode, wherein both light and external reduced carbon contribute to biomass accumulation. In this study, we investigated the consequences of mixotrophy on the growth and metabolism of the pennate diatom *Phaeodactylum tricornutum*, using glycerol as the source of reduced carbon. Transcriptomics, metabolomics, metabolic modelling and physiological data combine to indicate that glycerol affects the central-carbon, carbon-storage and lipid metabolism of the diatom. In particular, provision of glycerol mimics typical responses of nitrogen limitation on lipid metabolism at the level of TAG accumulation and fatty acid composition. The presence of glycerol, despite provoking features reminiscent of nutrient limitation, neither diminishes photosynthetic activity nor cell growth, revealing essential aspects of the metabolic flexibility of these microalgae and suggesting possible biotechnological applications of mixotrophy.

* To whom correspondence should be addressed: Dimitris.Petroutsos@cea.fr; Giovanni.Finazzi@cea.fr

Introduction

Diatoms are unicellular eukaryotes responsible for about 20-25% of the global carbon dioxide fixation *via* photosynthesis (photoautotrophy). Resulting from a secondary endosymbiotic event in which a red alga was engulfed by heterotrophic eukaryotic host, diatoms display a complex combination of genes and metabolic pathways acquired from endosymbiotic events and horizontal transfer with bacteria and viruses [1]. Ultimately, this chimeric metabolism is believed to be an essential component of the great evolutionary success [2,3] and the high biotechnological potential of these algae. The potential industrial uses of them include the utilization of their silica shell for nanostructures [4], food applications [5] and production of triacylglycerols (TAGs) for biofuel under low-input conditions [6]. Given their metabolic flexibility, different growth modes can be envoked in microalgae and diatoms in particular. The first is photoautotrophy, in which light energy directly fuels CO_2 conversion into reduced carbon *via* photosynthesis. This requires a photochemical conversion by the two photosystems (PSs), PSI and PSII, electron flow to generate reducing power (NADPH) and ATP, which are consumed for CO_2 uptake by Rubisco and the Calvin-Benson-Bassham (CBB) cycle.

The second mode is heterotrophy, in which algae grow in the absence of light by fermenting or respiring exogenous sugars [7]. Amongst the diatom heterotrophs, two different categories can be recognized: *i.* obligate heterotrophs (i.e. *Nitzschia alba*) that lack photosynthetic pigments and are thus not able to perform photosynthesis and *ii.* facultative heterotrophs (i.e. *Cyclotella cryptica*) that can separately perform photosynthesis and respiration. *C. cryptica* is able to grow in presence of glucose in the dark, but displays lower productivity than when operating in the photoautotrophic mode [8]. In fact, some microalgae are obligate photoautotrophs due to their possession of an inefficient uptake of carbon (reviewed in [9]). In keeping with this observation it was shown that introduction of the gene encoding for the human glucose transporter (GLUT1) in *P. tricornutum* allowed the uptake of glucose in the dark, thereby improving biomass production [10]. A third mode of cultivation is mixotrophy, *i.e.* the growth in presence of both light and organic carbon. This mode, which involves the utilization of respiration and photosynthesis simultaneously, is of particular interest to understand how the two major systems of energy metabolism harboured by plants and algae interact with one another. Various diatoms including *P. tricornutum* [11], *Navicula saprophila*, and some

2

species of *Nitzschia* [12] have been reported to grow mixotrophically, although with different efficiencies and substrate specificities. *N. saprophila* is able to grow in phototrophic mode as well as in presence of acetic acid, both in the presence or absence of light. However, the highest growth rate is observed when reduced carbon is added in the light (mixotrophy), roughly corresponding to the sum of the growth rates obtained in heterotrophy and phototrophy [12].

The model diatom *P. tricornutum* can grow on glycerol, acetate, glucose and fructose [11,13-15]. Recent results showing that diatoms optimise their photosynthetic efficiency *via* constitutive energetic interactions between mitochondria and plastids [16], have provided a molecular interpretation for mixotrophy. Indeed, coupling of respiratory and photosynthetic activities *via* exchanges of NADPH and ATP provides a tight coordination of these two processes, which should optimize utilization of light and reduced carbon by mixo-trophy. Since the metabolic consequences of mixotrophy are still poorly studied, we combined metabolic modelling, transcriptomics, metabolomics and lipidomics approaches with physiological measurements to provide a detailed picture of the metabolic changes induced by this growth mode in an attempt to propose possible future applications of this trophic mode in biotechnology.

Methods

Algal culture.

Strains and growth media. Axenic cultures of *P. tricornutum* (Pt1, CCAP 1055/3, [17]) were grown in 250 ml flask in artificial seawater ESAW [18] supplemented with additional $NaNO_3$ and NaH_2PO_4 to reach a final concentration of 0.47 g/L N and 0.03 g/L P (this medium will be referred as PHOT from now on). The-se elevated concentrations ensure that neither N nor P will be depleted during growth [19]. For N-depletion experiments, cells were shifted to an N-free medium (called here PHOT-N). Cells were grown in a chamber at 20°C, 40 μE m^{-2} s^{-1} irradiance with a 12-h-light / 12-h-dark photoperiod and shaking at 100 rpm. For mix-otrophic growth experiments, filter sterilized glycerol was added at a final concentration of 50 mM to both N-replete and N-deficient cultures, leading to the MIX and the MIX-N growth media, respectively.

To monitor algal growth, samples were taken daily (at the end of the light period) and growth was esti-mated by cell counting using a LUNA™ instrument (Logos Biosystems, Inc. USA). The initial inoculum was

0.5 and 2×10^6 cells/mL for N-replete and N-deplete condition respectively. Cells were collected after 5 days of growth for the various -omics analyses.

BiologTM plates assessment of growth and respiration. The effect of 190 different carbon sources on algal growth was screened to pinpoint possible candidates for mixotrophic cultivation of *P. tricornutum* using Phenotype Biolog MicroArrays™ [20]. This microplate assay is based on the use of 96-well plate containing pre-arrayed substrates such as carbohydrates, amino acids and carboxylic compounds. In this study, 2×10^6 cells/mL were resuspended in the PHOT medium [19] and 160 µL were deposited into each well. Growth was followed daily and substrates that improve growth were selected from a triplicate experiment. A few select metabolites were scaled up for use in 100 mL flasks. A phototrophic control was grown in parallel.

Nitrogen and phosphate concentration. Nitrogen and phosphate concentration were determined in the supernatant using test strips (Reflectoquant nitrate and phosphate), via a Merck RQflex reflectometer (E. Merck, 64271 Domsstadt, Germany). In the case of nitrogen, this approach was calibrated using a colorimetric assay kit to measure nitrite and nitrate (Sigma, USA), following the manufacturer instructions. In the case of phosphate, the method was calibrated according to [21].

Spectroscopy.

Chlorophyll Fluorescence Measurements. All the photosynthetic parameters were determined using a Speedzen MX fluorescence imaging setup (JBeamBio, France) as described in [22]. For each sample, 3 x 200 µl of algal culture, at a cell concentration of 1-5 million cells/mL, were transferred in a 24 well plate. The maximum quantum yield of PSII ($F_v/F_m = (F_m-F_0)/F_m$) was determined after 15 min of dark incubation, where F_m and F_0 are the maximum and minimum fluorescence of dark-adapted cells, respectively. Non-photochemical quenching (NPQ) was calculated as $(F_m-F_{m'})/F_{m'}$, where $F_{m'}$ and F_m are maximum fluorescence of light-adapted and dark-adapted cells respectively. Photosynthetic electron transfer rate (ETR) was calculated as $0.5 \times I \times Y(II)$, where 0.5 represents the fraction of light absorbed by PSII (half of the total incident light), I is the incident light intensity and Y(II) is the quantum yield of PSII in the light. The latter is defined as $(F_{m'}- F_{ss})/F_{m'}$, where F_{ss} is the fluorescence emission measured in the presence of the light [23].

4

Nile Red analysis. Accumulation of triacyglerols was monitored by Nile Red (Sigma-Aldrich) fluorescent staining as detailed in [19]. In brief, 40 µL of Nile Red dye (2.5 µg/mL stock concentration, in 100% DMSO) were added to 160 µL cell suspension (1-5 million cells/mL) in a 96-well white microplate and mixed. After 20 minutes of incubation at room temperature in the dark the Nile Red fluorescence was measured (530/580 nm: excitation/emission). Data were then normalized per million cells.

Metabolite analysis

Glycerol concentration. The glycerol concentration of 2 mL of filtered supernatant was evaluated using a Shimadzu HPLC equipped with a Hi-plex H+ (7.7 X 300 mm) Agilent column. The analysis was performed using the mobile phase 5 mM H_2SO_4. The detection wavelength was set at 880 nm using a RI RID-10A Detector with a flow rate of 0.6 mL/min and a temperature of 60°C. Peaks quantification was performed by comparison of a range of six standards.

Total lipid extraction. Total lipids were extracted according to [24]. About 20 mg of dried cells were homogenized with 1 mL of chloroform/methanol 2:1. The cells were then lysed using a TissueLyser II (Qiagen) with an agitation of 1 minute and a frequency of 300 s^{-1}. The lysate was washed with 200 µl of NaCl 0.9 % (v/w) and vortexed for some seconds in order to form the emulsion. The solution was centrifuged 5 min at 60,000 g to separate the two phases and the lower phase was placed in fresh pre-weighed glass tubes. The upper phase was washed with chloroform and subsequently lysis and centrifugation steps were repeated in order to recovery more lipids. The wash with chloroform was repeated at least twice. The lower phases (containing lipids) were collected in glass tubes and evaporated under a nitrogen stream at 65°C. The glass tubes were subsequently re-weighed to determine the percentage of lipids extracted per dry cell weight.

Separation by TLC, and Analyses by GC-FID and MS. Glycerolipids were extracted from lipid extract of *P. tricornutum* cells as described in [19]. To quantify the various classes of polar and non-polar glycerolipids, lipids were separated by TLC on glass-backed silica gel plates (Merck) using two distinct resolving systems [25]. To isolate nonpolar lipids including TAG and free FA, lipids were resolved by TLC run in one dimension with hexane:diethylether:acetic acid (70:30:1, v/v). Lipids were recovered from the silica powder

after the addition of chloroform:methanol (1:2, v/v) thorough mixing and collection of the chloroform phase [26]. Lipids were then dried under argon and either quantified by methanolysis and GC-FID of by MS.

Metabolite extraction and GC-MS Based Metabolite Profiling. Metabolites were extracted with some modifications of the protocol described in [27]. Ten-million cells were harvested on a Durapore-HV membrane filter disk of 2.5 cm diameter and 0.45 µm poresize (Millipore, Billerica, MA) by vacuum filtration. The filter with the cells was then transferred into a 1.5 ml tube and frozen in liquid nitrogen. Frozen samples were stored at −80 °C until metabolite extraction. Metabolites were extracted by immersing the filter in 1 ml of 90% (v/v) methanol containing 0.1 µg mL^{-1}. The tubes were sonicated in a water bath type sonicator for 1 min in ice cold water and then incubated at 4°C for 1 h with shaking. The remaining solution was centrifuged at 22,000 g for 5 min at 4 °C. A 50 µL aliquot of the supernatant was used for chlorophyll a determination whilst 900 µL was reduced to dryness using a vacuum concentrator (SpeedVac concentrator, Thermo, Waltham, MA). Dried samples were stored at −80 °C after filling the tubes with argon gas. The metabolite profile was determined exactly as described in [27].

Quantification of intracellular pyruvate. The concentration of pyruvate was evaluated by fluorescence-based method using the pyruvate assay kit (Cayman chemical).

Microarray analysis and statistics.

RNA extraction and gene expression analysis. Total RNA was extracted as described in [28]. Microarray processing and analysis was carried out onbiological triplicates as described in [29]. Microarray data have been deposited on the Gene Expression Omnibus (https://www.ncbit.nlm.nih.gov/geo/) under the accession GSE91004.

Statistical analysis. Data from the three independent experiments were tested for statistical significance of the variations in gene expression. This was determined using the -test implemented in MeV 4.9 [30]. The three independent replicates were used to perform a one-class analysis using a p Value of 0.01. A threshold of expression of absolute Log$_2$ (fold change) value > ± 0.75 was used to select genes differentially expressed between the test and the control conditions.

Mathematical Modelling.

Genome Scale Metabolic Model. A genome-scale metabolic model (GSM) of *P. tricornutum* was developed as described in (Singh, 2016 [31], starting from the model of [32]. The current model consists of 449 reactions, 140 transporters and 355 metabolites and is comprised of cytosolic, plastidial, mitochondrial and peroxisomal compartments. It can utilise NO_3, NH_4, SO_4, O_2, Pi and inorganic and/or organic carbon as input material for biomass production. It has been validated with respect to the laws of energy and mass conservation [33], and is able to produce all major biomass components (carbohydrate, lipid, amino acids, nucleotides etc.) in phototrophic and mixotrophic conditions in experimentally observed proportions.

Flux Balance Analysis. The model was analysed using a modification of Flux Balance Analysis (FBA) [34,35], in which the underlying linear program is repeatedly solved whilst increasing the constraint representing the photon input flux [36]. For this study, flux in glycerol uptake was increased instead of photon input flux and in addition, the proportions of individual biomass components were allowed to vary up to 5 fold. The FBA formulation is as follows:

$minimise: |v|$

subject to:

$$Nv = 0$$
$$v_\mu = \mu$$
$$t_{i..j} \leq v_{i..j} \leq s_{i..j}$$
$$v_{glycerol} = Glycerol$$
$$v_{ATPase} = ATPase$$
$$v_{LightCyc} \leq v_{LightNonCyc}$$
$$v_{carboxylase} + v_{oxygenase} \leq C \qquad \text{eq. 1.1}$$

where: the objective is to minimise total flux in the system.

N Is the stoichiometry matrix

v Is the rate vector

$Nv = 0$ Defines the steady-state constraint

v_μ defines the flux of photons (light intensity used in the experiment)

$v_{glycerol}$ defines the flux of glycerol into the system which was increased gradually.

$t_{i..j} \leq v_{i..j} \leq s_{i..j}$ Defines the range of allowable fluxes in the biomass transporters. The lower bound is the experimentally observed proportion and the upper bound is arbitrarily 5 times higher.

7

$v_{LightCyc} \leq v_{LightNonCyc}$ constraints the rate cyclic photophosphorylation to be no higher than that of non-cyclic.

$v_{carboxylase} + v_{oxygenase} \leq C$ Sets the upper limit on the sum of the rubisco carboxylase and oxygenase reactions. This can be regarded as proxy for overall limitation in the Calvin cycle. For this study, C = 0.8 mmol/ gDW * hr was based on the flux in rubisco reactions obtained in phototrophic condition with photon flux constrained to the experimental value.

Any solution to this equation thus generates a flux vector, v, describing the individual fluxes of reactions in the system at steady state growth with rates of production of biomass precursor defined by the flux values in $v_{i..j}$, the biomass transporters. In order to explore potential metabolic responses to increasing glycerol availability, Equation 1.1 was solved repeatedly whilst increasing $v_{glycerol}$ to represent increasing glycerol uptake. For this aspect of the study, the allowed photon flux into the system, v_{μ}, was constrained to be less than or equal to the light intensity used in the experiment and flux in glycerol transporter was varied from 0.01 to 1.0 mmol/gDW *hr (experimental glycerol consumption rate was estimated to be ≈ 0.1 mmol/ gDW * hr).

Results

Consequences of mixotrophic growth on biomass production in *P. tricornutum* cells. As a first step to investigate the effect of external reduced carbon sources, we measured growth and physiological properties of cells in Erlenmeyer flasks in cells of the pennate diatom *P. tricornutum*. Experiments were performed in the PHOT medium to avoid nitrogen and phosphorous starvation during growth [19]. Glycerol was chosen as the respiratory substrate, as its consequences on metabolism have been already studied to some extent in this alga, and its low cost makes it a suitable substrate for possible future exploitation for biotechnology [11,37]. When tested in 50 mL Erlenmeyer flasks, glycerol enhanced biomass production by a factor of two as compared to growth on PHOT medium (Fig. 1A). Its effect was gradual, given the progressive consumption of this compound by the algae (Fig. 1B), and became clearly visible after 5 days of growth.

The enhanced growth capacity observed in glycerol supplemented cells resulted in a much faster consumption of nitrogen (Fig. 1C) and phosphate (Fig. 1D), leading to a complete depletion by the end of the growth phase. Given that nutrient starvation (nitrogen starvation in particular) affects photosynthesis [38,39], we looked for possible effects of glycerol on photosynthetic parameters, measuring the quantum yield of PSII (F_v/F_m), the electron flow between PSII and PSI (ETR), and the photoprotective responses of the cells, as indicated by the NPQ parameter. We found (Fig. 2), that glycerol addition had only minor effects on photosynthesis not only at the beginning of the experiment (day one), but also at day five, *i.e.* after the consequences of this compound on growth become evident, as well as at the end of the growth experiment (day 10). As a corollary of this experiment, we confirmed the large decrease in photosynthesis in *P. tricornutum* cells upon transfer to -N that we had previously observed in [19].

Flux Balance Analysis of the *P. tricornutum* metabolic network. Since the glycerol-mediated improvement of biomass productivity in *P. tricornutum* is not due to a direct effect on photosynthesis, we explored its effect on other areas of cellular metabolism. For this purpose, FBA was performed on the GSM of *P. tricornutum* as described in the Methods. The number of reactions in the solution to equation 1.1, varied between 339 and 353 over the range of imposed glycerol uptake rates. The greatest variations were in the CBB cycle, tricarboxylic acid (TCA) cycle, Oxidative Pentose Phosphate Pathway (OPPP), mitochondrial electron transport chain (mETC), photorespiration, glycolysis, lipid synthesis, carbohydrate synthesis and lactate excretion. Flux in reactions associated with the CBB, including that of Rubisco and CO_2 uptake decreased with glycerol uptake. By contrast, flux in reactions associated with photorespiration, the TCA cycle, glycolysis, OPPP and photorespiration increased with glycerol uptake. Fluxes in lipid and carbohydrate synthesis reactions increased leading to increased production of these classes of storage compound. An increased excretion of lactate was also observed with glycerol uptake. The reactions that showed more than 1% variation, in response to glycerol uptake, form a connected subnetwork depicted in Fig.3.

Organic and inorganic carbon were utilised when glycerol was assumed to be available. As shown in Fig.3, CO_2 is fixed by the RuBP carboxylase reaction (r1 in Fig. 3) which drives the CCB cycle and thereby contributes towards biomass production. Glycerol is converted to glycerol-3P by glycerol kinase (r48). It can be used as the glycerol-backbone for TAG synthesis and/or is further degraded to DHAP by glycerol-3-

9

P dehydrogenase (r49). DHAP can be utilised for X5P and R5P production which can be converted to RuBP and enter the CCB cycle orphotorespiration. It can also be utilised for pyruvate production *via* glycolysis or can be converted to F6P and G6P *via* reactions FBPaldol (r5), FBPase (r6) and G6Piso (r8) which may *via* subsequent reactions contribute towards an increase in carbohydrate production. Pyruvate can be fermented to lactate *via* Lacdh (r52) and/or it can be utilised for AcCoA production by Pyrdh (r21). It can also be converted by pyruvate carboxylase (r34) to OAA which can then enter the TCA cycle or be utilised *via* threonine metabolism (r36-r39).

The RuBP oxygenase reaction (r50) is active and glycolate produced as a consequence is subsequently metabolised to glyoxylate and thereafter utilised by the glyoxylate shunt of the TCA cycle. Gly and Ser produced during the process are metabolised to PGA *via* reactions of glycerate metabolism (r40-r45). Reactions involved with (internal) HCO_3^- fixation namely PEPCarboxylase (r35) and pyruvate carboxylase (r34), as well as the TCA cycle and mETC, including the alternative oxidase, are also active.

Metabolic and transcriptomic assessment of glycerol-mediated changes in *P. tricornutum* cells. To verify our model predictions, we experimentally assessed changes in metabolic pathways. Consistent with our prediction, previous results indicate that glycerol affects the cellular lipid content [37]. We confirmed this result by measuring TAG accumulation using Nile Red fluorescence (Fig. 4A-B). We found that in nitrogen rich medium the presence of glycerol enhanced Nile Red fluorescence at day 5. The choice of day 5 to perform metabolic analyses is justified by the need to measure changes at the earliest stage of the glycerol response, to avoid artefacts related to cell ageing and/or consumption of other nutrients. Indeed, nutrient starvation, that of nitrogen in particular, largely increases the accumulation of TAGsin microalgae [40,41]. Thus, day 5, which represents the first data point where significant glycerol effects on growth are detected (Fig. 1), was the ideal time point to perform a detailed analysis.

The finding that glycerol increases Nile Red fluorescence even in N supplemented cells suggests that TAG accumulation is also increased by this compound in N replete conditions. This conclusion was further substantiated by the quantification of total lipid content (Fig. 4C), and of the DAG and TAG fractions (Fig. 4D-E) by mass spectrometry. We found that the TAG content was specifically increased by glycerol (Fig. 4E), in agreement with the Nile Red observations, in both nitrogen replete and starved cells. As expected,

we also observed that nitrogen starvation not only induced a substantial TAG accumulation, but also enhanced the total lipid content. Conversely, glycerol addition did not modify this parameter significantly (Fig. 4C). In parallel to the changes in the TAG content, we found that the TAG fatty acid (FA) composition was modified by glycerol. In particular, C16:0 and C16:1 FA were higher in glycerol grown cells (Supplementary Fig. 1), suggesting that this compound induces *de novo* biosynthesis of FA [19,25]. Glycerol also promoted accumulation of long chain FAs (*i.e.* 20:5) that usually correspond to lipids obtained from recycling of membrane lipids, as suggested by the decrease of the phosphatidylcholine (PC) most abundant phospholipid species found in extraplastidic membranes of eukaryotic cells [42]. (Supplementary Fig. 1 and 2, respectively). The increase of C20:5 has already been reported following N limitation in *P. tricornutum*. Thus, we conclude that glycerol addition affects lipid metabolism by mimicking most of the effects of nitrogen limitation [19], although clearly to a lesser extent. However, at variance with N limitation, the addition of glycerol had a positive effect on growth (Fig. 1A).

To better understand the effect of glycerol on cellular metabolism, we next compared the metabolite profiles of cells grown in the absence (PHOT) and presence (MIX) of this compound. Whilst the levels of most of the metabolites analysed by GC-MS were not affected by glycerol addition, a few of them displayed significant changes. In particular, six metabolites (lactate, xylose, trehalose, docosahexaenoic acid; DHA and mannitol) were increased by glycerol while four (valine, alanine, guanidine and leucine) were decreased by this compound (Fig. 5). The changes of lactate, valine, alanine and leucine suggest that glycerol could affect the pyruvate hub (Fig. 6). Given that this metabolite could not reliably be measured *via* GC-MS, to test this possibility, we directly quantify the pyruvate content in the same cell extracts using a commercial kit (Supplementary Fig. 3). We found that glycerol addition increased the pyruvate content, suggesting a higher flux from glycerol to the pyruvate. The finding that pyruvate was increased likely provides a rationale for the increased respiratory activity in cells gown on glycerol, measured by a polarographic approach (Supplementary Fig. 4). On the other hand, the decrease in alanine, leucine and valine all of which derive from pyruvate was somewhat unexpected.

The complementary changes in trehalose and mannitol also point to a change in carbon storage metabolism (Fig. 6). The change in DHA is compatible with the modifications observed by lipidomic analysis. To

11

corroborate the hypothesis that glycerol affects primary, storage carbon and lipid metabolisms, we additionally performed a comparative transcriptomic analysis on microarray using RNA from cultures grown for 5 days in the presence or absence of glycerol. Statistical analysis on the microarray data revealed 35 genes to be differentially expressed in the presence of glycerol (Table I). Notably, most of these genes encode proteins involved in lipid, amino acid and glycolytic metabolism (Table I), consistent with our conclusions concerning central carbon metabolism, lipid biosynthesis and storage derived from our metabolite analyses (Fig. 6).

Finally, the results obtained with glycerol lead us to explore if other compounds could be used as substrates to boost biomass production in microalgae. To identify new substrates, we grew *P. tricornutum* cells in Biolog™ plates PM1 and PM2A, supplemented with 190 different carbon sources, for 6 days. This allowed monitoring biomass productivity (*via* cell counting). We found that several compounds, not previously identified as mixotrophic substrates for *P.tricornutum* enhanced growth of *P. tricornutum* cells (Supplementary Fig. 5). They include fumarate, aspartate, asparagine and serine. Despite the clear benefit of glycerol on growth of *P.tricornutum* in flasks (Fig. 1A, Supplementary Fig. 5B and C), this compound did not improve growth at the microplate scale (Supplementary Fig. 5A). This observation may be due to a lower oxygen availability in the microwells circumventing the efficient respiration observed upon glycerol addition to liquid cultures (Supplementary Fig 3). However, for the compounds which enhanced growth in the microplate scale enhanced growth could be confirmed also in liquid cultures, confirming the utility of this approach in pinpointing biotechnologically relevant mixotrophic substrates.

Discussion

Metabolic consequences of glycerol mediated mixotrophic growth. The metabolic flexibility of diatoms has often been invoked to explain their evolutionary success. Indeed, these algae can grow in different modes: photosynthetically, simply converting the sunlight energy into reduced carbon *via* photosynthesis or heterotrophically via sugar fermentation in the dark. This mode of growth is however not possible in *P. tricornutum*, which can use sugars in the dark only upon metabolic engineering [10]. On the other hand, *P. tricornutum* can grow mixotrophically, *i.e.* simultaneously using light and reduced carbon [11,37]. Here, we

12

have investigated the metabolic consequences of glycerol addition on *P. tricornutum* cells, finding that this compound promotes higher growth and modifies the metabolism in terms of accumulation of carbon resources, including lipids and other carbon storage compounds. The results obtained from the modelling investigation allow the identification of the pathways most likely to be involved in this process.

Photorespiration. The glycerol metabolism of *P. tricornutum* was previously investigated, using isotope labelling experiments with ^{13}C-glycerol as carbon source [43,44]. These studies highlighted that under mixotrophic conditions *P. tricornutum* cells mostly convert this compound into Gly and Ser. A similar observation was made in our modelling analysis. As shown in Fig. 3, photorespiration is active and the glycolate produced by the RuBP oxygenase reaction can be metabolised to Gly and Ser. The *P. tricornutum* metabolic network has confirmed the capability to produce Gly and Ser from both photorespiratory and non-photorespiratory routes [45]. However, an interesting observation is that the model suggests the latter route is used under conditions of high glycerol availability. Previous analysis of this model [31] suggests that photorespiration becomes active as a result of supra-optimal light intensities. The increased photorespiratory flux is associated with increased fluxes towards Gly and Ser.

On the other hand, no significant changes were observed in the cellular levels of serine and glycine in our experimental analysis, despite the fact that the levels of several other amino acids displayed significant changes following the addition of glycerol. The relationship between the concentration of a metabolite and the fluxes of the reactions in which it is involved is complex and potentially counter intuitive. However, it is possible to say that if the activity of all reactions in a given pathway increase proportionately then the fluxes of those reactions will increase by the same proportions while the concentrations of the intermediate metabolites will remain unaffected [46]. For instance, it is possible that the enhanced flux towards Gly and Ser evaluated by others [43,47] and predicted by our model cannot lead to any measurable changes in the concentration of these amino acids, likely because of a tight coupling between production and consumption of these compounds. Consequently, there is no inherent inconsistency between the experimental and the model results reported here.

Effect of glycerol on carbon metabolism. On the other hand, other metabolic changes were pinpointed by our comparison of light and light + carbon driven growth, using complementary approaches (lipidomics,

13

transcriptomics and metabolomics). After 5 days of growth, the majority of the differentially regulated genes encode proteins associated with carbon and lipid metabolism. This result suggests that glycerol induces a specific modification of cellular metabolism in order to cope with the increased availability of carbon. The extra energy flux provided by the glycerol to cells grown in non-limiting light conditions (Fig.1A, 0 to 5 days) is possibly diverted to storage, as confirmed by Nile Red staining (Fig. 3A, B). Genes encoding factors involved in cell regulatory process and cell cycle progression were unaffected in cells grown under mixotrophic as opposed to phototrophic growth conditions. Given that glycerol has a clear effect on growth, we can speculate that these genes were differentially regulated in the first days following glycerol addition, but that their expression level had returned to normal by treatment day 5 which we investigated here. Most importantly we strongly believe that the observed changes in central-carbon, carbon-storage and lipid metabolismin mixotrophycally vs phototropically grown *P. tricornutum* cells are consistent with the modelling results.

In the modelling results, glycerol enters central carbon metabolism *via* its conversion to glycerol phosphate by glycerol kinase and thereafter by glycerol 3 phosphate dehydrogenase to DHAP. This is consistent with the observed effects of overexpression of two enzymes involved in glycolysis and gluconeogenesis namely TPI (*PHATR_50738*) and FBPac5 (*PHATR_51289*) in the microarray analysis (table I). The higher level of pyruvate (Supplementary Fig. 3) can be explained by the higher glycolytic flux. Modelling suggests that pyruvate can be fermented to lactate *via* LDH, act as a substrate for lipid synthesis or be converted *via* pyruvate carboxylase to OAA which enters the TCA cycle. The latter route is supported by the experimentally observed increase in lactate concentration data and the increased respiratory rate.

The modelling results also suggest increased fluxes to storage carbohydrate in the presence of glycerol. This too, is consistent with our experimental data, although we additionally observed an increase in trehalose and mannitol, and not just chrysolaminarin as predicted by the model analysis. This finding suggests that besides chrysolaminarin, which is the most abundant carbohydrate storage form in diatoms [48], *P. tricornutum* can accumulate, at least to some extent, other storage sugars when provided with external organic carbon. Consistent with this, *P. tricornutum* possesses a complete set of enzymes for the biosynthesis of trehalose and mannose and we observed that one of them was up-regulated by glycerol (*i.e.*

14

GDP-mannose 4,6-dehydratase, *PHATR_25417)*. Moreover, we identified a putative mannitol dehydrogenase in the genome of *Phaeodactylum* (*i.e. PHATH_*30246) that is involved in the conversion of the mannose into mannitol. This gene showed some homology (c. 37, 2%) with the mannose dehydrogenase enzyme M1PDH from the brown algae *Ectocarpus siliculosus*. Both the trehalose and mannitol pathway have been already identified in brown algae, where they appear to have been inherited from the red algal progenitor and *via* lateral gene transfer from *Actinobacteria* respectively [49]. Thus, it seems reasonable to assume that a similar situation may be present in *P. tricornutum*. Alternatively, it is conceivable that the observed changes in mannitol and threalose upon addition of glycerol represent a response to an increased osmotic pressure induced by this compound. Consistent with this idea, previous data in both prokaryotes and eukaryotes [50-52], have shown that both trehalose and mannitol are induced by osmotic stress.

Our experimental analysis also points to glycerol mediated effects on lipid metabolism, consistent with previous reports [11]. Our modelling results suggests that glycerol can be metabolized to contribute to TAG biosynthesis by providing the glycerol-backbone as well as providing substrates for FA biosynthesis, producing the acyl groups required for TAG assembly (Fig. 6). These results are also corroborated by our microarray analysis, which reveals an up-regulation of the fatty acids desaturases *ptd9 (PHATR_ 28797)* as well as the acetyl-transferase *dagat2d* (*PHATR_* 43469) involved in the FA and TAG biosynthesis, respectively. Moreover, our analysis of the FA composition of TAGs in glycerol treated cells suggests that their accumulation is due to *de novo* synthesis as well as to the degradation of some pre-existing membrane lipids. In general, TAGs can be produced by two main routes: *i. de novo* synthesis of fatty acids directly incorporated into TAGs *via* the Kennedy pathway involving a diacylglycerol acyltransferase and *de novo* DAG and acetyl-CoA synthesis (*e.g.* [19,25]), or *ii.* conversion of pre-existing polar glycerolipids [53]. TAGs generated by the first route contain newly generated fatty acids, *i.e.*, high levels of C16:0 and C16:1 FAs. Conversely, TAGs obtained from recycling of membrane lipids contain fatty acids with a substantial proportion of elongated and polyunsaturated molecular species such as C20:5 fatty acids. Our data (Supplementary Fig. 1) indicate that glycerol-grown cells contain a higher amount of 16:0 and 16:1 fatty acids, consistent with the occurrence of *de novo* synthesis. However, glycerol also leads to an increased accumula-

15

tion of C20:5 fatty acids, consistent with the occurrence of some membrane lipid turnover. This behaviour is very similar to that observed in *P. tricornutum* cells upon exposure to nitrogen starvation [19]. However, in contrast with N limited cells, glycerol supplemented cells do not display *i.* any significant degradation of the most abundant thylakoids lipids, *i.e.* MGDG and DGDG (Supplementary Fig. 2), or *ii.* any loss of photosynthetic activity (Fig. 2). Thus, although the consequences of glycerol addition of lipids are reminding of those of nitrogen starvation [19] in terms of TAG accumulation and changes in the fatty acids profile, this compound seems to act mainly at the level of lipid biosynthesis rather than degradation.

The model analysis highlights possible changes in flux distribution in the metabolic network and changes in biomass composition, again consistent with our experimental observations. However, FBA and related approaches do not fully explain changes in the steady-state concentration of internal metabolites. One of the routes for alanine synthesis is the reversible transamination of pyruvate and following simple logic one would expect to see an increase in alanine co-incident with an increase in pyruvate. Similarly, pyruvate is also the carbon precursor of valine and leucine in the chloroplast and an increase in these amino acids was also expected. A possible explanation for the observed decrease in valine and leucine concentration would be to assume a heterogeneous distribution of pyruvate in the cells. As FA synthesis is boosted in the presence of glycerol and *de novo* FA biosynthesis occurs in the chloroplast, it might be that while pyruvate increases globally at the cellular level (explaining the increased levels in Supplementary Fig. 3), its concentration could be lower in the chloroplast, because of efficient consumption by the plastidial pyruvate dehydrogenase during FA synthesis. An increased availability of glycerol 3-phosphate for lipid synthesis might also effectively "drain" the FA biosynthetic pathway. This could relieve product inhibition of pyruvate dehydrogenase, ultimately reinforcing pyruvate consumption in the chloroplast.

Effect of glycerol on biomass productivity. Glycerol addition leads to a substantial increase in growth in Phaeodactylum (Fig. 1). However, a careful analysis of its effects on growth reveals that not all the glycerol provided to the cells is converted into biomass. While almost $1gL^{-1}$ of glycerol was consumed during algal cultivation (Fig. 1B), the cell number was increased from $5*10^5$ cells L^{-1} to $2*10^7$ cells L^{-1}. Based on the relationship between cell number and biomass (DCW) in our samples, this corresponds to around 0.6 g L^{-1} of biomass increase. Thus, the consumption of glycerol does not directly match to the increase of biomass.

16

The model results, described above, provide a potential resolution to this apparent contradiction: as the rate of glycerol uptake was increased, there was a decrease in the CBB cycle. Furthermore, the calculated fluxes in the mitochondria responded to increased glycerol uptake in a broadly opposite sense to those of the CBB cycle, leading to an increased production of CO_2. Both these responses resulted in a reduction of net CO_2 fixation in the model, and this provides a working hypothesis to explain the difference between the experimental consumption of glycerol and increase in biomass.

Conclusion

This work highlights the potential of mixotrophic growth for biotechnology applications. Indeed, mixotrophy can enhance biomass productivity while providing advantages in terms of lipid accumulation, which are normally seen under nutrient starvation. While glycerol induces some responses typical of nitrogen limited cells with regard to TAG accumulation (Fig. 4) and FA composition (Supplementary Fig. 1), no inhibition of the photosynthetic capacity of the cell is seen in the presence of this compound (Fig. 2).

By revealing the main metabolic pathways targeted by glycerol, our work also suggests possible targets for metabolic engineering. For instance, inhibition of the biosynthesis of storage carbohydrates could potentially divert carbon (derived from glycerol) towards TAG production. This was observed in our model analysis and also already reported in the case of the main sugar storage polymer, chrysolaminarin [54]. It is hoped that ongoing integration of our data into a mathematical model could reveal other possible target to further increase the algal production capabilities.

The observed capacity to use glycerol supplied in the medium suggests the existence a glycerol transporter (most likely an aquaporin type transporter). The identification and characterization of such system would have relevant consequences to understand its role in natural conditions (the ocean water are often enriched in organic carbon due to the relatively high turnover of the plankton components) and inspire biotechnological developments. The parallel use of engineered strains and new substrates for growth (Supplementary Fig. 5) could largely improve biomass productivity in mixotrophically grown microalgae.

Abbreviations

RuBP: ribulose-1,5-bisphosphate, PGA: 3-phospho-D-glycerate, 2PG: 2-phosphoD-glycerate, PEP: phosphoenol pyruvate, Pyr: pyruvate, X5P: xylulose-5-phosphate, GAP: glyceraldehyde 3-phosphate, Pi: phosphate, AcCoA: acetyl-CoA, Ser: serine, Gly: glycine, , Acet: acetate, AcAld: acetate-aldehyde, THR: threonine, ASP: aspartate, OAA: oxaloacetatic acid, 2KG: 2-ketoglutarate, GLT: glutamate, Glyox: glyoxylate, SBP: sedoheptulose-1,7-bisphosphate, 6PG: 6phosphogluconate, FBP: fructose bisphosphate, E4P: erythrose-4-phosphate, F6P: fructose-6-phosphate, DHAP: dihydroxyacetone phosphate, S7P: sedoheptulose7-phosphate, R5P: ribose-5-phosphate, BPGA: 1,3-diphosphateglycerate, G6P: glucose-6-phosphate, G1P: glucose-1-phosphate, ATP: adenosine-triphosphate, ADP: adenosine-diphosphate, 6PG: 6-phosphogluconate, Pyr: pyruvate, Mal: malate, Fum: fumarate, Cit: citrate, Suc: succinate, NAD: nicotinamide adenine dinucleotide, NADP: nicotinamide adenine dinucleotide phosphate, IsoCit: isocitrate, SucCoA: succinyl-S-CoA, SucAld: succinic semialdehyde, OH-Pyr: 3-hydroxypyruvate, Q: ubiquinone, QH2: ubiquinol, Cyt red: Cytochromes-CReduced, Cyt ox: Cytochromes-C-Oxidized, rubisco: RuBP carboxylase/oxygenase, , FBPase: fructose 1,6-bisphosphatase, FBPaldol: FBP aldolase, , Pyrdh: Pyruvate dehydrogenase, Glycerol-3P: glycerol-3-phosphate , G6Piso: G6P isomerase, Lacdh: Lactate dehydrogenase, TPI: Triosephosphate isomerase, DHA: docosahexaenoic acid, TAG: triacylglycerol, FA: fatty acid; ALA: alanine, LEU: leucine, VAL: valine, EPA: eicosapentaenoic acid, fbac5: fructose bisphosphate aldolase, dagat2d:Diacyl Glycerol acyltransferase 3 phosphate, gmd: GDP-mannose 4,6-dehydratase, ptd9: fatty acids desaturases 9, M1PDH: mannose 1-phosphate dehydrogenase, PUFA: polyunsaturated fatty acid.

Additional Information

References

1. Armbrust, E. V. 2009 The life of diatoms in the world's oceans. *Nature* **459**, 185–192.

2. Thomas, D. N. & Dieckmann, G. S. 2002 Antarctic Sea ice--a habitat for extremophiles. *Science* **295**, 641–644.

3. Hutchins, D. A., DiTullio, G. R., Zhang, Y. & Bruland, K. W. 1998 An iron limitation mosaic in the California upwelling regime. *Limnol. Oceangr.* **43**, 1037–1054.

4. Lechner, C. C. & Becker, C. F. W. 2015 Silaffins in silica biomineralization and biomimetic silica precipitation. **13**, 5297–5333.

5. Vinayak, V., Manoylov, K. M., Gateau, H. L. N., Blanckaert, V., Herault, J., Pencreach, G. L., Marchand, J., Gordon, R. & Schoefs, B. T. 2015 Diatom milking? A review and new approaches. **13**, 2629–2665.

6. Chisti, Y. 2007 Biodiesel from microalgae. *Biotechnol Adv* **25**, 294–306.)

7. Lewin, J. C. & Lewin, R. A. 1960 AUXOTROPHY AND HETEROTROPHY IN MARINE LITTORAL DIATOMS. *Can. J. Microbiol.* **6**, 127–134.

8. Hellebust, J. A. 1971 GLUCOSE UPTAKE BY CYCLOTELLA CRYPTICA: DARK INDUCTION AND LIGHT INACTIVATION OF TRANSPORT SYSTEM 2. *Journal of Phycology* **7**, 345–349.

9. Chen, G. Q. & Chen, F. 2006 Growing phototrophic cells without light. *Biotechnol Lett* **28**, 607–616.

10. Zaslavskaia, L. A., Lippmeier, J. C., Kroth, P. G., Grossman, A. R. & Apt, K. E. 2001 Transformation of the diatom Phaeodactylum tricornutum (Bacillariophyceae) with a variety of selectable marker and reporter genes. *Journal of Phycology* **36**, 379–386.

11. Ceron Garcia, M. C., Garcia Camacho, F., Miron, A. S., Sevilla, J. M. F., Chisti, Y. & Molina Grima, E. 2006 Mixotrophic production of marine microalga Phaeodactylum tricornutum on various carbon sources. *J. Microbiol. Biotechnol.* **16**, 689–694.

12. Kitano, M., Matsukawa, R. & Karube, I. 1997 Changes in eicosapentaenoic acid content of Navicula saprophila, Rhodomonas salina and Nitzschia sp. under mixotrophic conditions. *J Appl Phycol* **9**, 559–563.

13. Ceron Garcia, M. C., Fernandez-Sevilla, J. M., Fernández, F. G. A., Molina Grima, E. & Garcia Camacho, F. 2000 Mixotrophic growth of Phaeodactylum tricornutum on glycerol: growth rate and fatty acid profile. *J Appl Phycol* **12**, 239–248.

14. Liu, X. J., Duan, S. S., Li, A. F. & Sun, K. F. 2009 Effects of glycerol on the fluorescence spectra and chloroplast ultrastructure of Phaeodactylum tricornutum (Bacillariophyta). *J Integr Plant Biol* **51**, 272–278.

15. Haiying Wang 2012 A study on lipid production of the mixotrophic microalgae Phaeodactylum tricornutum on various carbon sources. *Afr. J. Microbiol. Res.* **6**.

16. Bailleul, B. et al. 2015 Energetic coupling between plastids and mitochondria drives CO2 assimilation in diatoms. *Nature* **524**, 366–369.

17. Martino, A. D., Meichenin, A., Shi, J., Pan, K. & Bowler, C. 2007 Genetic and phenotypic characterization of Phaeodactylum tricornutum (Bacillariophyceae) accessions. *Journal of Phycology* (doi:10.1111/j.1529-8817.2007.00384.x)

18. Berges, J. A., Franklin, D. J. & Harrison, P. J. 2001 Evolution of an Artificial Seawater Medium: Improvements in Enriched Seawater, Artificial Water Over the Last Two Decades. *Journal of Phycology* **37**, 1138–1145.

19. Abida, H. et al. 2015 Membrane glycerolipid remodeling triggered by nitrogen and phosphorus starvation in Phaeodactylum tricornutum. *Plant Physiol.* **167**, 118–136.

20. Bochner, B. R. 2003 New technologies to assess genotype–phenotype relationships. *Nat. Rev. Genet.* **4**, 309–314.

21. Lanzetta, P. A., Alvarez, L. J., Reinach, P. S. & Candia, O. A. 1979 An improved assay for nanomole amounts of inorganic phosphate. *Analytical Biochemistry* **100**, 95–97.

22. Johnson, X., Vandystadt, G., Bujaldon, S., Wollman, F. A., Dubois, R., Roussel, P., Alric, J. & Beal, D. 2009 A new setup for in vivo fluorescence imaging of photosynthetic activity. *Photosynth Res* **102**, 85–93.

23. Maxwell, K. & Johnson, G. N. 2000 Chlorophyll fluorescence--a practical guide. *J. Exp. Bot.* **51**, 659–668.

24. Folch, J., Less, M. & Sloane Stanley, G. H. 1957 A simple method for the isolation and purification of total lipides from animal tissues. *J. Biol. Chem.* **226**, 497–509.

25. Simionato, D., Block, M. A., La Rocca, N., Jouhet, J., Marechal, E., Finazzi, G. & Morosinotto, T. 2013 The response of Nannochloropsis gaditana to nitrogen starvation includes de novo biosynthesis of triacylglycerols, a decrease of chloroplast galactolipids, and reorganization of the photosynthetic apparatus. *Eukaryot Cell* **12**, 665–676. (doi:10.1128/EC.00363-12)

26. Bligh, E. G. & Dyer, W. J. 1959 A rapid method of total lipid extraction and purification. *Canadian Journal of Biochemistry and Physiology* **37**, 911–917.

27. Obata, T., Schoenefeld, S., Krahnert, I., Bergmann, S., Scheffel, A. & Fernie, A. R. 2013 Gas-Chromatography Mass-Spectrometry (GC-MS) Based Metabolite Profiling Reveals Mannitol as a Major Storage Carbohydrate in the Coccolithophorid Alga Emiliania huxleyi. *Metabolites 2013, Vol. 3, Pages 325-346* **3**, 168–184.

28. Huysman, M. J. J. et al. 2013 AUREOCHROME1a-mediated induction of the diatom-specific cyclin dsCYC2 controls the onset of cell division in diatoms (Phaeodactylum tricornutum). *Plant Cell* **25**, 215–228.

29. Fortunato, A. E. et al. 2016 Diatom Phytochromes Reveal the Existence of Far-Red-Light-Based Sensing in the Ocean. *Plant Cell* **28**, 616–628.

30. Eisen, M. B., Spellman, P. T., Brown, P. O. & Botstein, D. 1998 Cluster analysis and display of genome-wide expression patterns. *Proc. Natl. Acad. Sci. U.S.A.* **95**, 14863–14868.

31. Singh, D., Carlson, R., Fell, D. & Poolman, M. 2015 Modelling metabolism of the diatom Phaeodactylum tricornutum. *Biochem. Soc. Trans.* **43**, 1182–1186.

32. Hunt, K. A., Folsom, J. P., Taffs, R. L. & Carlson, R. P. 2014 Complete enumeration of elementary flux modes through scalable demand-based subnetwork definition. *Bioinformatics* **30**, 1569–1578.

33. Gevorgyan, A., Poolman, M. G. & Fell, D. A. 2008 Detection of stoichiometric inconsistencies in biomolecular models. *Bioinformatics* **24**, 2245–2251.

34. Varma, A. & Palsson, B. O. 1993 Metabolic capabilities of Escherichia coli: I.

cofactors. *J. Theor. Biol.* **165**, 477–502.

35. Varma, A. & Palsson, B. Ø. 1993 Metabolic Capabilities of Escherichia coli II. Optimal Growth Patterns. *J. Theor. Biol.* **165**, 503–522. (doi:10.1006/jtbi.1993.1203)

36. Poolman, M. G., Kundu, S., Shaw, R. & Fell, D. A. 2013 Responses to light intensity in a genome-scale model of rice metabolism. *Plant Physiol.* **162**, 1060–1072.

37. Ceron Garcia, M. C., Fernandez-Sevilla, J. M., Sanchez Miron, A., Garcia Camacho, F., Contreras-Gómez, A. & Molina Grima, E. 2013 Mixotrophic growth of Phaeodactylum tricornutum on fructose and glycerol in fed-batch and semi-continuous modes. *Bioresour. Technol.* **147**, 569–576.

38. Saha, S. K., Uma, L. & Subramanian, G. 2003 Nitrogen stress induced changes in the marine cyanobacterium Oscillatoria willei BDU 130511. *FEMS Microbiology Ecology* **45**, 263–272.

39. Li, Y., Horsman, M., Wang, B., Wu, N. & Lan, C. Q. 2008 Effects of nitrogen sources on cell growth and lipid accumulation of green alga Neochloris oleoabundans. *Applied Microbiology and Biotechnology* **81**, 629–636.

40. Cakmak, T., Angun, P., Demiray, Y. E., Ozkan, A. D., Elibol, Z. & Tekinay, T. 2012 Differential effects of nitrogen and sulfur deprivation on growth and biodiesel feedstock production of Chlamydomonas reinhardtii. *Biotechnol. Bioeng.* **109**, 1947–1957.

Alonso, D. L., Belarbi, E. H., Fernandez-Sevilla, J. M., Rodriguez-Ruiz, J. & Molina Grima, E. 2000 Acyl lipid composition variation related to culture age and nitrogen concentration in continuous culture of the microalga Phaeodactylum tricornutum. *Phytochemistry* **54**, 461–471.

42. Henneberry, A. L., Lagace, T. A., Ridgway, N. D. & McMaster, C. R. 2001 Phosphatidylcholine synthesis influences the diacylglycerol homeostasis required for SEC14p-dependent Golgi function and cell growth. *Mol. Biol. Cell* **12**, 511–520.

43. Zheng, Y., Quinn, A. H. & Sriram, G. 2013 Experimental evidence and isotopomer analysis of mixotrophic glucose metabolism in the marine diatom Phaeodactylum tricornutum. *Microb. Cell Fact.* **12**, 109.

44. Huang, A., Liu, L., Yang, C. & Wang, G. 2015 Phaeodactylum tricornutum photorespiration takes part in glycerol metabolism and is important for nitrogen-limited response. *Biotechnol Biofuels* **8**, 73.

45. Bromke, M. A. 2013 Amino Acid biosynthesis pathways in diatoms. *Metabolites 2013, Vol. 3, Pages 325-346* **3**, 294–311.

46. Kacser, H. & Burns, J. A. 1973 The control of flux. *Symp. Soc. Exp. Biol.* **27**, 65–104.

47. Kim, J., Fabris, M., Baart, G., Kim, M. K., Goossens, A., Vyverman, W., Falkowski, P. G. & Lun, D. S. 2015 Flux balance analysis of primary metabolism in the diatom Phaeodactylum tricornutum. *Plant J.* **85**, 161–176.

Kroth, P. G. et al. 2008 A model for carbohydrate metabolism in the diatom Phaeodactylum tricornutum deduced from comparative whole genome analysis. *PLoS ONE* **3**, e1426.

49. Michel, G., Tonon, T., Scornet, D., Cock, J. M. & Kloareg, B. 2010 Central and storage carbon metabolism of the brown alga Ectocarpus siliculosus: Insights into the origin and evolution of storage carbohydrates in Eukaryotes. *New Phytol*

50. Domínguez-Ferreras, A., Soto, M. J., Pérez-Arnedo, R., Olivares, J. & Sanjuán, J. 2009 Importance of trehalose biosynthesis for Sinorhizobium meliloti Osmotolerance and nodulation of Alfalfa roots. *J. Bacteriol.* **191**, 7490–7499.

51. Tekolo, O. M., Mckenzie, J., Botha, A. & Prior, B. A. 2010 The osmotic stress tolerance of basidiomycetous yeasts. *FEMS Yeast Research* **10**, 482–491.

52. Sugawara, M., Cytryn, E. J. & Sadowsky, M. J. 2010 Functional role of Bradyrhizobium japonicum trehalose biosynthesis and metabolism genes during physiological stress and nodulation. *Appl. Environ. Microbiol.* **76**, 1071–1081.

53. Li-Beisson, Y. et al. 2013 Acyl-lipid metabolism. *Arabidopsis Book* **11**, e0133.

54. Daboussi, F. et al. 2014 Genome engineering empowers the diatom Phaeodactylum tricornutum for biotechnology. *Nat Comms* **5**, 3831.

Tables

Table I. Relevant genes regulated in mixotrophic growth. The table shows the genes selected by t-test analysis in microarray analysis that significantly changed (Log2 fold change> ±0.75, p value < 0.01) in transcript abundance between mixotrophic and phototrophic conditions. In the case of genes related to carbon metabolism sub-cellular localization prediction using ChloroP, TargetP (Emanuelsson et al., 2007) and ASAFind (Gruber et al., 2015) is reported. Expression values are the average of three biological replicates ± SD. Chloro: chloroplast localization; Mito: mitochondrial localization; np: negative prediction.

21

Figure captions

Fig.1 Growth curves and nutrients consumption of _Phaeodactylum tricornutum_. A. Growth curves of _P. tricornutum_ cells in N-replete and N-deplete condition in the presence/absence of glycerol. Two different starting cell density were used in N-replete and N-deplete condition: 10^6 cells/mL and $2x10^6$ cells/mL respectively. B. Glycerol consumption of _P. tricornutum_ cells in N-replete conditions. C. Nitrate and D. phosphate consumption kinetics in _P. tricornutum_ cultures in N-replete condition in the presence/absence of glycerol; Each result is the average of two biological replicates ± SD. PHOT: light in N-replete condition; PHOTO-N: light in N-deplete condition; MIX: light+glycerol in N-replete condition; MIX-N: light+glycerol in N-deplete condition.

Fig.2 Photosynthetic activity in _P. tricornutum_. A. Photosynthetic efficiency represented as Fv/Fm ratio; B. Non-photochemical quenching (NPQ) and C. Electron transport rate (ETR) of cells cultivated for 5 and 10 days in N- replete or N- deplete conditions in both phototrophic and mixotrophic mode. Each result is the average of two biological replicates ± SD. PHOT: light in N-replete condition; PHOTO-N: light in N-deplete condition; MIX: light+glycerol in N-replete condition; MIX-N: light+glycerol in N-deplete condition.

Fig 3 The network composed of reactions exhibiting change in flux in response to increase glycerol uptake. In order to understand the potential metabolic response in presence of glycerol, Flux Balance Analysis, with minimisation of sum of absolute fluxes as objective function along with biomass production constraint, was performed repeatedly with gradual increase in glycerol uptake. This analysis was used to identify reactions with co-related response to change in glycerol uptake in presence of light. Reactions r1-r20: Calvin cycle/Glycolysis/Gluconeogenesis, r21: Pyrdh, r22-r32: TCA cycle, r33-r35: C4 metabolism, r36-r40: Thr metabolism, r41-r45: Glycerate metabolism, r46-r47: Oxidative pentose phosphate pathway, r48-49: Glycerol degradation, r50: RuBP oxygenase, r51: Glycolate oxidase, r52: LHD, I-V:ETC, AOX: Alternative oxidase, L1-L2: Light reactions. Reactions with increased flux is denoted by green while those with reduced flux is denoted by red. Note: Flux in RuBP carboxylase decreases however flux in most of the reactions involved with Calvin cycle increases as they are also associated with other metabolic routes. External metabolites are denoted in the boxes, CO2 and O2 are considered to be exchanged between the organism and the medium.

Fig.4 Glycerolipid production in _P. tricornutum_. A. Epifluorescence images of cells, at their 5th day of growth, stained with Nile Red dye. B. Neutral lipid content normalized per millions of cells determined by Nile Red staining at day 5 and 10. C. Total lipids accumulation at day 5 in _P. tricornutum_ expressed as percentage of dry weight. D. DAG and E. TAG accumulation at day 5 in _P. tricornutum_ normalized per mg of dry cells. Each result is the average of two biological replicates ± SD. PHOT: light in N-replete condition; PHOTO-N: light in N-deplete condition; MIX: light+glycerol in N-replete condition; MIX-N: light+glycerol in N-deplete condition.

Fig.5 Metabolomic analysis of _P. tricornutum_ grown in N-replete condition. The ratio log2 mixo/photo> 0 (green spots) represents all the metabolites that were over-expressed in mixotrophy in replete condition, while the ratio log2 mixo/photo< 0 (red spots) the metabolites down-regulate in this condition. Each result is the average of six biological replicates

Fig. 6 Hypothetical mode of action of glycerol supply on metabolism and mixotrophic growth of *Phaeodacty-lum*. The supply of glycerol can impact on A. central carbon, B. storage carbon and C. lipid metabolism during the mixotrophic growth of *Phaeodactylum*. Glycerol likely fuels the lower part of glycolysis, followed by the acetyl-CoA and TAG productions and the upper part of gluconeogenesis, followed by carbohydrate production. Italic green type represents gene transcripts found to be up-regulated in presence of glycerol in microarray analysis. Gene ID numbers are also indicated. Bold green or red type represents metabolites that were detected in the current study by GC-MS analysis in cells grown in mixotrophy or phototrophy respectively. The pyruvate was detected by "Pyruvate Assay Kit" and TAG in lipidomics analysis. Glyc3P: glycerol 3 phosphate; DHAP: dihydroxyacetone phosphate; GAP: glyceraldehyde-3 phosphate; FA: fatty acid; ALA: alanine; LEU: leucine; VAL: valine; F6P: fructose-6-phosphate; G6P: glucose-6 phosphate; EPA: eicosapentaenoic acid; DHA: docosahexaenoic acid; *tpi*: Triose phosphate isomerase; *fbac5*: fructose bisphosphate aldolase; *dagat2d*: Diacyl Glycerol acyltransferase 3 phosphate, *gmd*: GDP-mannose 4,6-dehydratase, *ptd9*: fatty acids desaturases 9.

Supplementary Fig. 1 Quantitative analysis of *P. tricornutum* glycerolipids. TAG profile in a total lipid extract from cells grown in replete conditions (A) and deplete conditions (B) in both mixotrophic and phototrophic mode. Glycerolipids are expressed in nmol / mg of dry cells. Each result is the average of two biological replicates ± SD. PHOT: light in N-replete condition; PHOTO-N: light in N-deplete condition; MIX: light+glycerol in N-replete condition; MIX-N: light+glycerol in N-deplete condition.
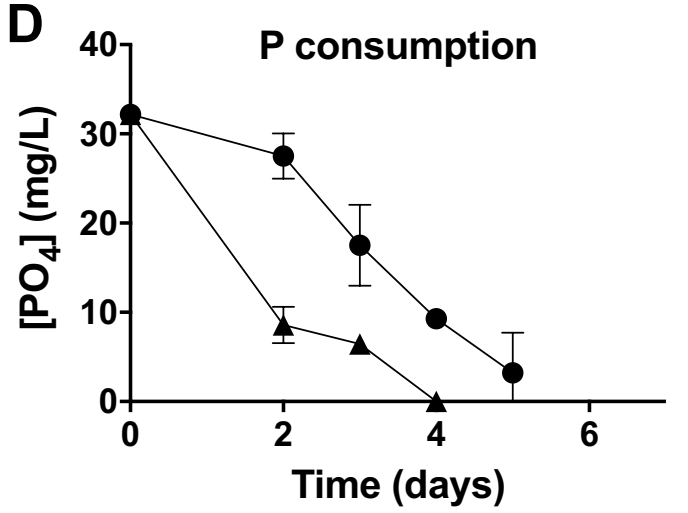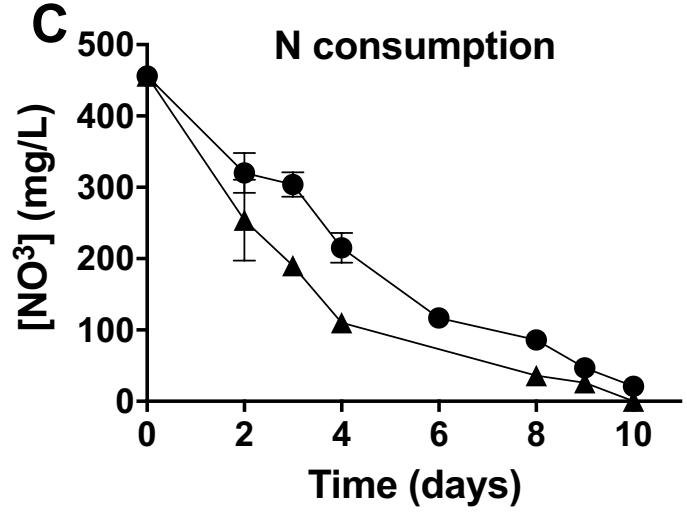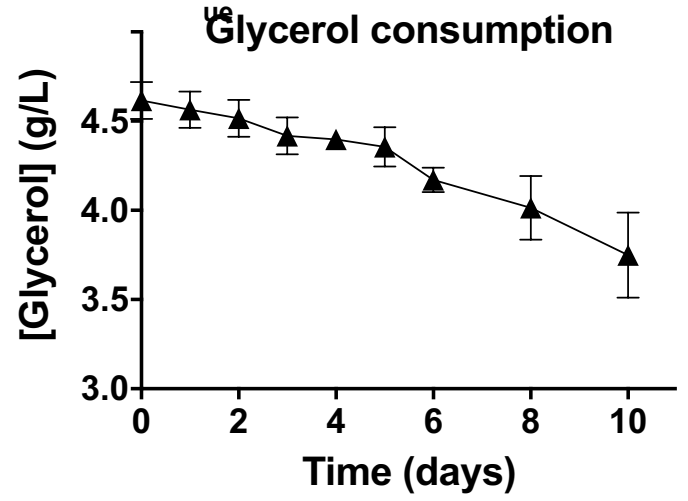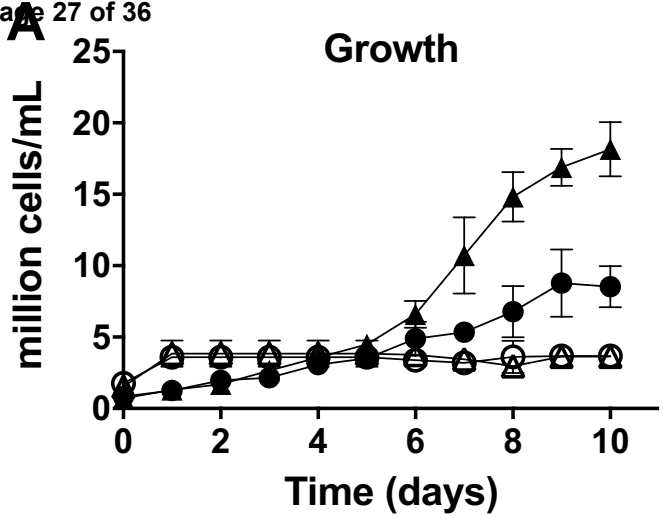
Supplementary Fig. 2 Membrane lipid composition in *P. tricornutum*. Lipid analysis of cells grow in N-replete conditions and N-deplete conditions in both mixotrophic and phototrophic mode. Each result is the average of two biological replicates ± SD. SQDG, sulfoquinovosyldiacylglycerol; DGDG, digalactosyldiacylglycerol; MGDG, monogalactosyldiacylglycerol; PC, phosphatidylcholine; PHOT: light in N-replete condition; PHOTO-N: light in N-deplete condition; MIX: light+glycerol in N-replete condition; MIX-N: light+glycerol in N-deplete condition

Supplementary Fig. 3 Quantification of intracellular pyruvate by a fluorescence-based method. A. Pyruvate standard curve. B. Quantification of intracellular pyruvate in cells grown in phototrophy (PHOT) and mixotrophy (MIX).
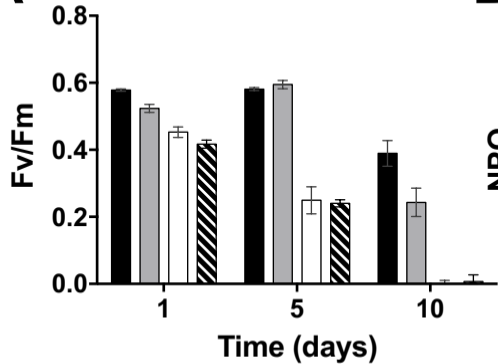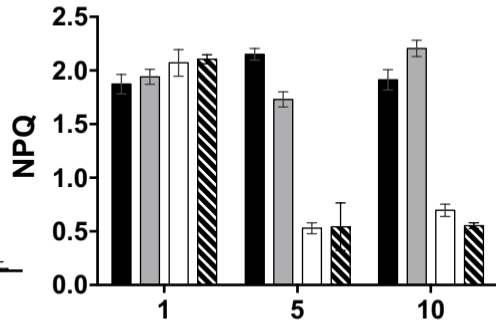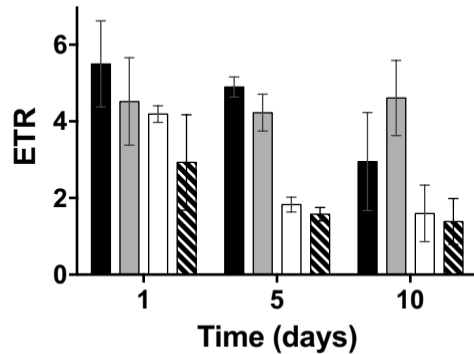
Supplementary Fig. 4 A Respiration and photosynthesis in *P. tricornutum* cells. Direct assessment of oxygen consumption by a polarographic approach in both phototrophy (black bar) and mixotrophy (red bar). B. Fluorescent based-assay to monitoring the changes in respiration using the Redox Dye A in presence of the selected compounds (see methods).

Supplementary Fig. 5 Screening of mixotrophic efficiency by biolog and redox dye assay in *P. tricornutum*. A. $OD_{750\ nm}$ changes (relative to phototrophic growth) of *P. tricornutum* cells grown for 6 days in BiologTM plates P1 and PM2A that contains 190 carbon compounds (see methods). Each data point represents a different compound. B. Growth profile of *P. tricornutum* on few selected compounds (at 20 mM) and a phototrophic control in 100 mL flasks. C. Areas under the growth curves of Supplementary Fig. 5B normalized to the area of the curve of phototrophic growth.
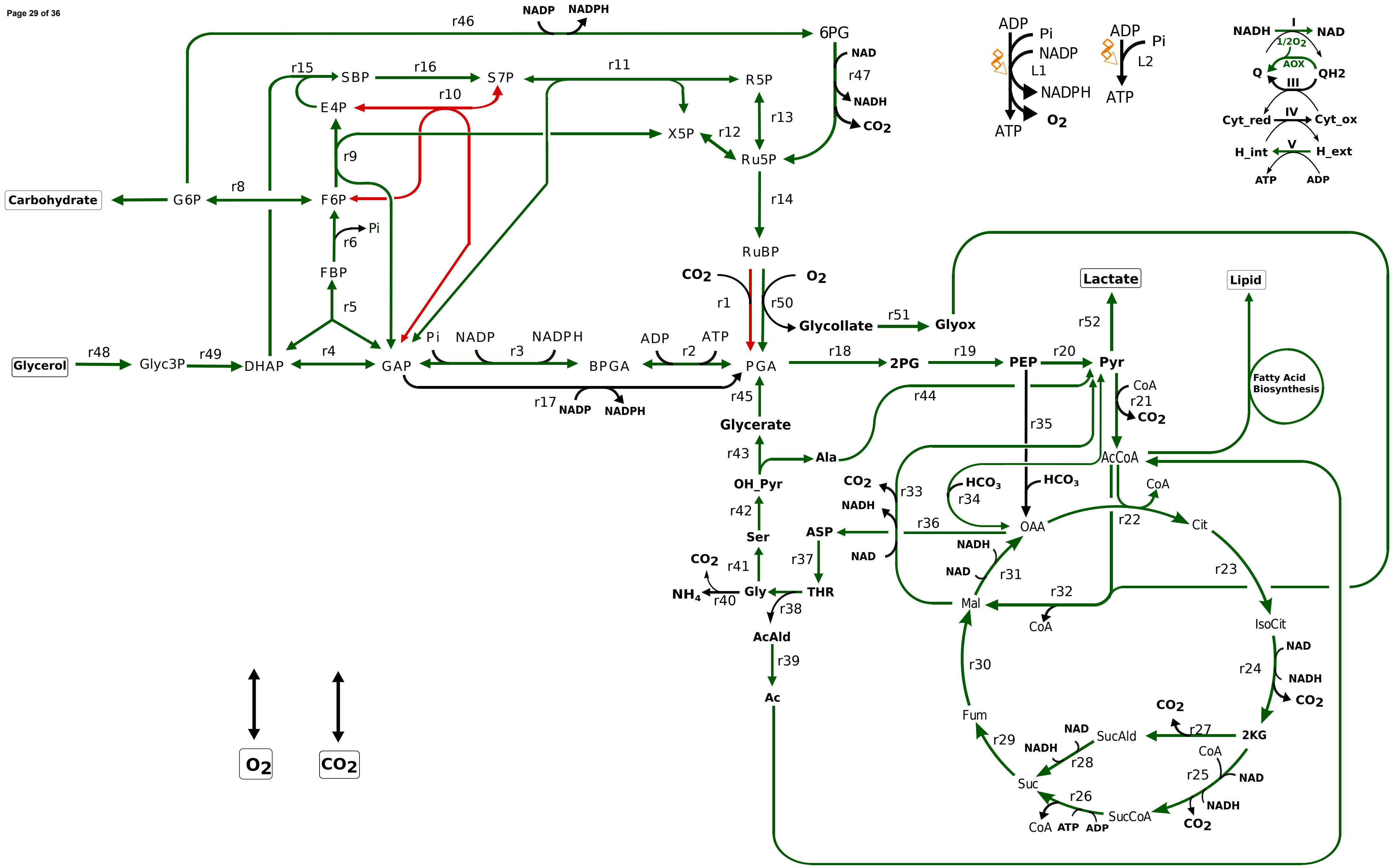
24

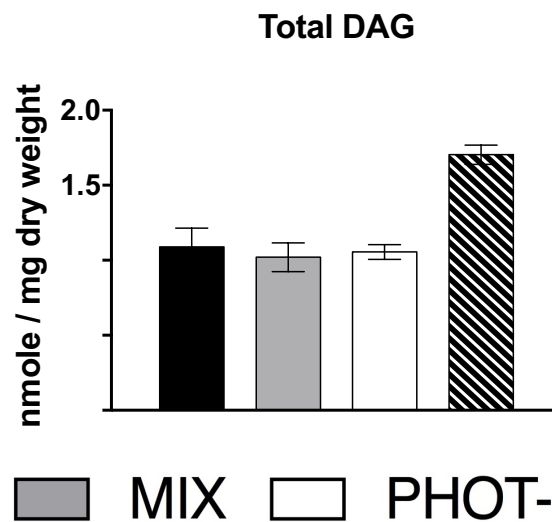| Gene Id (version2)	Gene Id (version 3)	Gene Expression (Log$_2$)	Std. Dev.	Annotation	pathway	Chloro P/ Target P prediction	ASAFind prediction
Phatr2_49283	Phatr3_J49283	3.08	0.44	Predicted protein			
Phatr2_42882	Phatr3_J42882	2.34	0.52	Predicted protein			
Phatr2_28797	Phatr3_J28797	2.27	0.20	stearoyldesaturase (delta9desaturase)	EPA biosynthesis	others	np
Phatr2_33087	Phatr3_J33087	1.61	0.26	Predicted protein			
Phatr2_46822	Phatr3_J46822	1.58	0.14	P-loop containing nucleoside triposphate hydrolase			
Phatr2_51289	Phatr3_J51289	1.58	0.30	FbaC5 (fructose-bisphosphate aldolase)	glycolysis	chloro	plastid, low confidence
Phatr2_30967	Phatr3_J30967	1.50	0.24	ketol acid reducto isomerase	super pathway leucine, valine	chloro	plastid, low confidence
Phatr2_50738	Phatr3_J50738	1.46	0.22	Triosephosphate isomerase	glycolysis	chloro	plastid, low confidence
Phatr2_48920	Phatr3_J48920	1.67	0.01	fibrillarin			
Phatr2_43961	Phatr3_J43961	1.44	0.22	alpha/beta hydrolase fold			
Phatr2_31718	Phatr3_J31718	1.26	0.16	Inosine-5'-monophosphate dehydrogenase	Urate biosynthesis	others	np
Phatr2_44522	Phatr3_J44522	1.10	0.13	Predicted protein			
Phatr2_43703	Phatr3_J43703	1.04	0.14	oxoglutarate/iron-dependent dioxygenase			
Phatr2_40998	Phatr3_J40998	1.03	0.06	Zinc finger C2H2			
Phatr2_31878	Phatr3_J31878	1.02	0.16	CAM2 (calmodulin)			
Phatr2_45855	Phatr3_J45855	1.00	0.10	NTF2-like domain (PF07080)			
Phatr2_25417	Phatr3_J25417	0.92	0.08	Glucose/ribitol dehydrogenase (PF00106)	GDP-L-Fucose biosynthesis I	others	np
Phatr2_9983	Phatr3_J9983	0.87	0.13	50S ribosomal protein L30e-like (PF01248)			
Phatr2_45509	Phatr3_J45509	0.84	0.05	Carbon-nitrogen hydrolase (PF00759)			
Phatr2_43469	Phatr3_J43469	0.83	0.14	DGAT2D - Diacylglycerol acyltransferase	Kennedy pathway	secretory	np
Phatr2_43024	Phatr3_J43024	0.77	0.04	tetratricopeptide repeat (PF13424)			
Phatr2_32629	Phatr3_J32629	-0.75	0.08	Predicted protein			
Phatr2_46117	Phatr3_J46117	-0.77	0.10	Predicted protein			
Phatr2_15806	Phatr3_J15806	-0.78	0.09	PDS-like3, Phytoene desaturase-like, phytoene dehydrogenase-like			
Phatr2_47655	Phatr3_J47655	-0.79	0.06	endoribonuclease L-PSP/chorismate mutase-like (PF14588)			
Phatr2_31876	Phatr3_J31876	-0.98	0.12	reverse transcriptase RNA-dependent DNA polymerase (PF07727)			
Phatr2_48291	Phatr3_J48291	-1.02	0.10	EF-hand domain (PF13499)			
Phatr_1199	Phatr3_J1199	-1.04	0.15	Leucine-rich repeat (PF13516)			
Phatr2_48021	Phatr3_J48021	-1.04	0.15	Predicted protein			
Phatr2_2164	Phatr3_J2164	-1.12	0.27	D-xylose:proton symporter	xylose degradation	secretory	np
Phatr2_42568	Phatr3_EG02435	-1.15	0.18	helicase-associated (PF03457)			
Phatr2_44192	Phatr3_EG02162	-1.23	0.19	Predicted protein			
Phatr2_40368	Phatr3_J40368	-1.30	0.12	Predicted protein			
Phatr2_38713	Phatr3_J38713	-1.70	0.26	Ribonuclease H-like domain			
Phatr2_46275	Phatr3_J46275	-2.29	0.25	HYP (FA desaturase type 1 domain)	unknown	others	np

A Growth

B Glycerol consumption

C N consumption

D P consumption

PHOT ● MIX ▲ PHOT-N ○ MIX-N △

Figure: Scatter plot of $\log_2$ mix/phot versus Metabolites. Data points labelled include lactate (~10, green), xylose (green), DHA (green), threalose (green), mannitol (green), valine (red), alanine (red), leucin (red), guanidin (red, gray).

B. Storage carbon metabolism

GLUCONOGENISIS

Trehalose biosynthesis

G6P → → **TREHALOSE**

(fbac5, PHATR_51289)

F6P → MAN ⇢ **MANNITOL**

GPD-Mannose biosynthesis
(*gmd, PHATR_25417*)

GLYCEROL → GLYC3P → DHAP ⇄ GAP

Kennedy pathway

(d*agat2d, PHATR_ 43469)*

(*tpi, PHATR_*50738)

GLYCOLYSIS

ALA, LEU, VAL
(*kari, PHATR_30*967)

Superpathway Amino acids

PYRUVATE → **LACTATE**

Lactate fermentation

TCA CYCLE

TAG

Acyl-coa ← **FA**

A. Central carbon metabolism

C. Lipid metabolism

(EPA, **DHA**)

A

B

C